CHAPTER IV
RESULTS AND DISCUSSION

4.1 Hydrogen Desorption of $Mg(BH_4)_2$

4.1.1 Synthesis of $Mg(BH_4)_2$

To synthesize $Mg(BH_4)_2$, a mixture of $LiBH_4$ and $MgCl_2$ was prepared with a 2:1 molar ratio by the ball-milling technique at 2 and 5 h. The XRD patterns in Figure 4.1 provide the phase of the $LiBH_4/MgCl_2$ mixture milled for 2 and 5 h and $LiBH_4$ milled for 5 h. The XRD patterns of the $LiBH_4/MgCl_2$ mixture milled for 2 and 5 h (Figure 4.1(b) and 4.1(c)) consist of Li_2MgCl_4 and LiCl peaks whereas the peaks corresponding to $LiBH_4$ (Figure 4.1(a)) and $MgCl_2$ disappear. It can be deduced that the ball milling process induces $LiBH_4$ to react with $MgCl_2$ through the following reaction (Matsunaga *et al.*, 2008):

$$2LiBH_4 + MgCl_2 \rightarrow Mg(BH_4)_2 + 2LiCl \qquad (4.1)$$

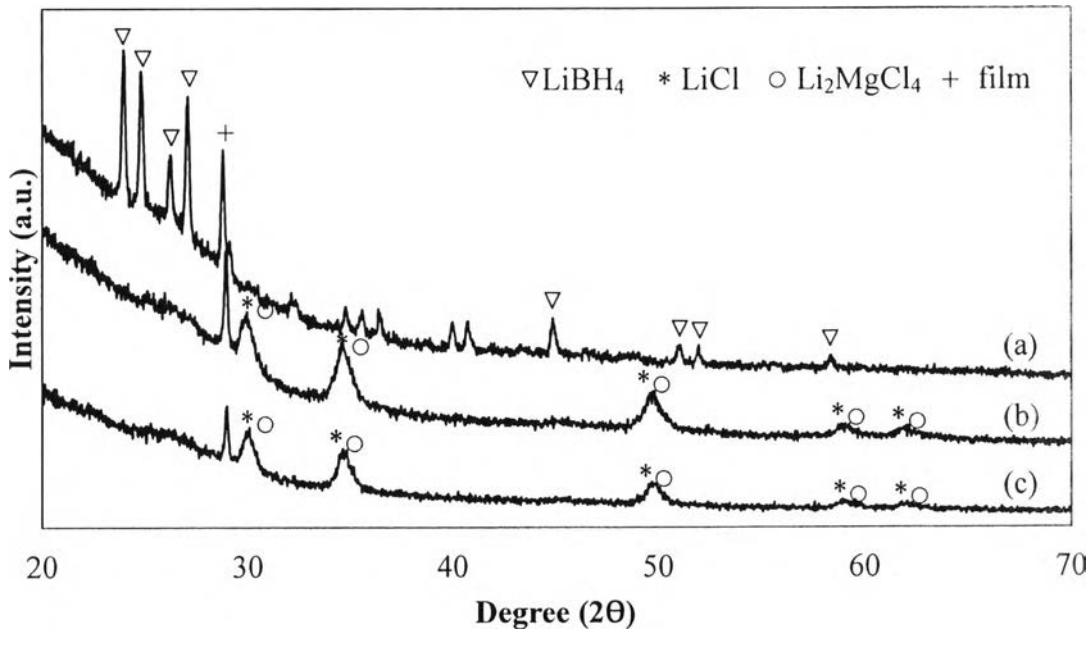

Figure 4.1 X-ray diffraction patterns of $LiBH_4$ milled for 5 h (a), the $LiBH_4/MgCl_2$ mixture milled for 2 h (b) and 5 h (c).

Comparison between the XRD patterns of the $LiBH_4/MgCl_2$ mixture milled for 2 and 5 h shows that the intensity of the sample ball milled for 5 h (Figure 4.1(c)) is lower than that ball milled for 2 h (Figure 4.1(b)). That is believed to be contributed from the partial decomposition of the $LiBH_4/MgCl_2$ mixture to LiCl and H_2 during the ball milling process. Therefore, the ball milling time of 2 h is expected to be adequate to synthesize $Mg(BH_4)_2$.

The reason for the absence of a diffraction pattern of $Mg(BH_4)_2$ may be that the compound synthesized by the ball milling method is not crystallized sufficiently (Li *et al.*, 2008). Furthermore, Varin *et al.* (2010) reported that ball milling of $LiBH_4$ with $MnCl_2$ resulted in the formation of a new complex metal borohydride, and the XRD pattern of the $LiBH_4/MnCl_2$ mixture after ball milling showed the strong diffraction peaks of LiCl.

The DSC profiles of the $LiBH_4/MgCl_2$ mixture after ball milling for 2 h are shown in Figure 4.2. Profiles of $LiBH_4$ and $MgCl_2$ after ball milling for 2 h were also investigated as references. For $LiBH_4$ (Figure 4.2(a)), there are endothermic peaks at 114 °C and 292 °C corresponding to the phase transition of $LiBH_4$, whereas no peak is observed for the $LiBH_4/MgCl_2$ mixture in this temperature range. For $MgCl_2$ (Figure 4.2(b)), the DSC profile shows an endothermic peak at 300 °C and there is no peak of the $LiBH_4/MgCl_2$ mixture in this temperature range. This result implies that the reaction between $LiBH_4$ and $MgCl_2$ takes place during the ball milling and the endothermic peaks of the $LiBH_4/MgCl_2$ mixture are similar to the decomposition temperature of $Mg(BH_4)_2$ (Matsunaga *et al.*, 2008 and Li *et al.*, 2008). Therefore, the DSC results support that $Mg(BH_4)_2$ was synthesized by the ball milling.

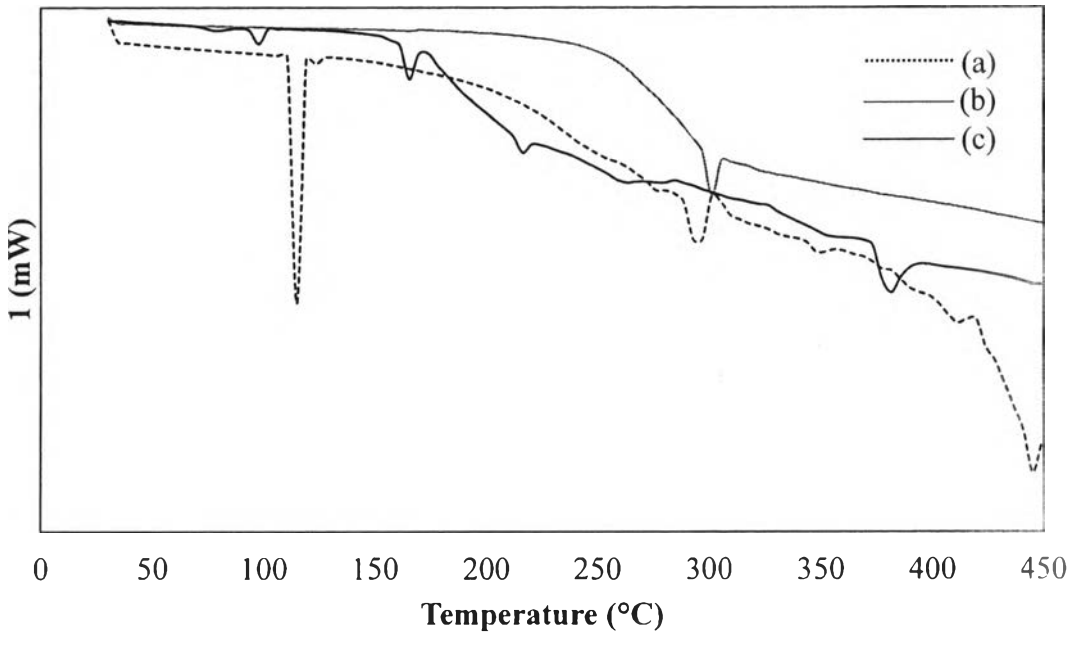

Figure 4.2 Differential scanning calorimetry profiles of $LiBH_4$ (a), $MgCl_2$ (b), and the $LiBH_4/MgCl_2$ mixture (c) milled for 2 h.

4.1.2 Hydrogen Desorption of $Mg(BH_4)_2$

The hydrogen desorption profiles of $Mg(BH_4)_2$ at different ball milling times are presented in Figure 4.3. For the ball milling time of 2 h (Figure 4.3(a)), $Mg(BH_4)_2$ starts to decompose at 30 °C. The first desorption step occurs at 214 °C and releases about 2.43 wt% hydrogen. The second step releases 2.10 wt% hydrogen and takes place at 374 °C, with the total amount of 4.78 wt% hydrogen. Similar results were obtained from $Mg(BH_4)_2$ ball milled for 5 h (Figure 4.3(b)). It starts to release hydrogen at 61 °C, while the starts of the first and second desorption are at 226 °C and 374 °C with the accumulated hydrogen of 1.97 wt% and 2.56 wt%, respectively. The total amount of desorbed hydrogen is about 4.76 wt% hydrogen. These results indicate the hydrogen desorbs in the following two steps (Matsunaga *et al.*, 2008):

$$Mg(BH_4)_2 \rightarrow MgH_2 + 2B + 3H_2 \qquad (1^{st} \text{ step}) \qquad (4.2)$$

$$MgH_2 \rightarrow Mg + H_2 \qquad (2^{nd} \text{ step}) \qquad (4.3)$$

Moreover, the results indicate that the mixing between $LiBH_4$ and $MgCl_2$ to synthesize $MgBH_4$ results in the decrease in the desorption temperature compared to $LiBH_4$ that shows the starting desorption temperature at 300 °C and the first desorption step at 380 °C (Figure 4.3(c)). However, $LiBH_4$ shows higher hydrogen capacity, about 6.55 wt% hydrogen.

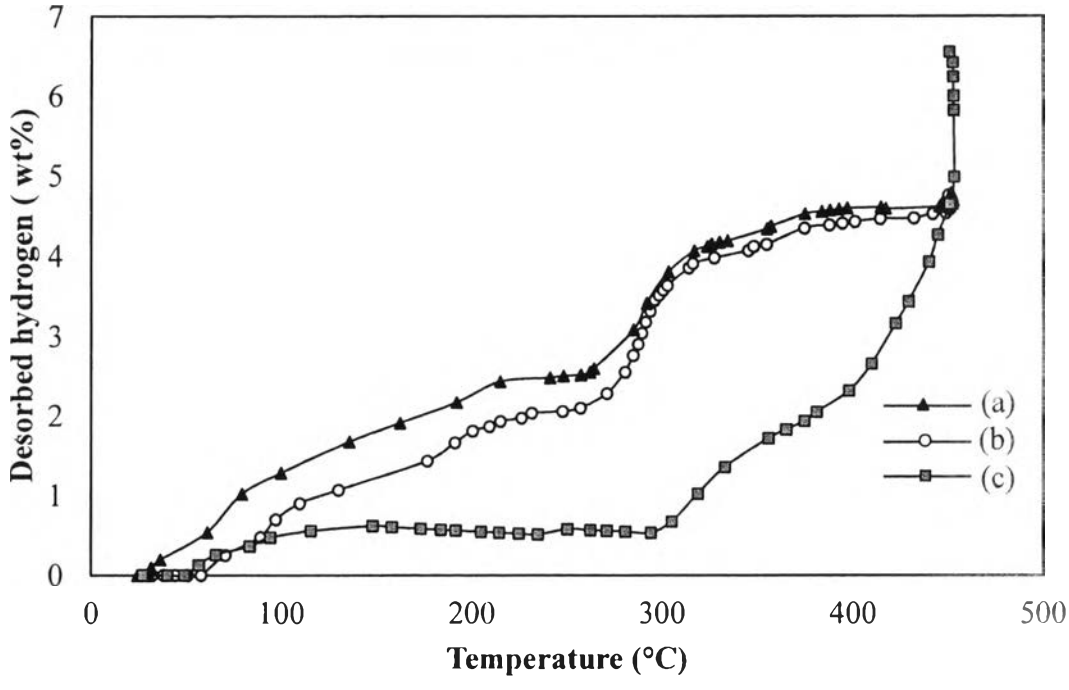

Figure 4.3 Hydrogen desorption profiles of the $LiBH_4/MgCl_2$ mixture milled for 2 h (a) and 5 h (b) and $LiBH_4$ milled for 5 h (c).

The DSC profiles in Figure 4.4 show the phase transformation temperature of the $LiBH_4/MgCl_2$ mixture milled for 2 and 5 h. The DSC profile of the $LiBH_4/MgCl_2$ mixture milled for 2 h (Figure 4.4(a)) shows the first step of hydrogen desorption temperature at 212 °C and the second step at 377 °C. For the mixture ball milled for 5 h (Figure 4.4(b)), the result shows hydrogen desorption temperature of the first and second steps at 244 °C and 380 °C, respectively.

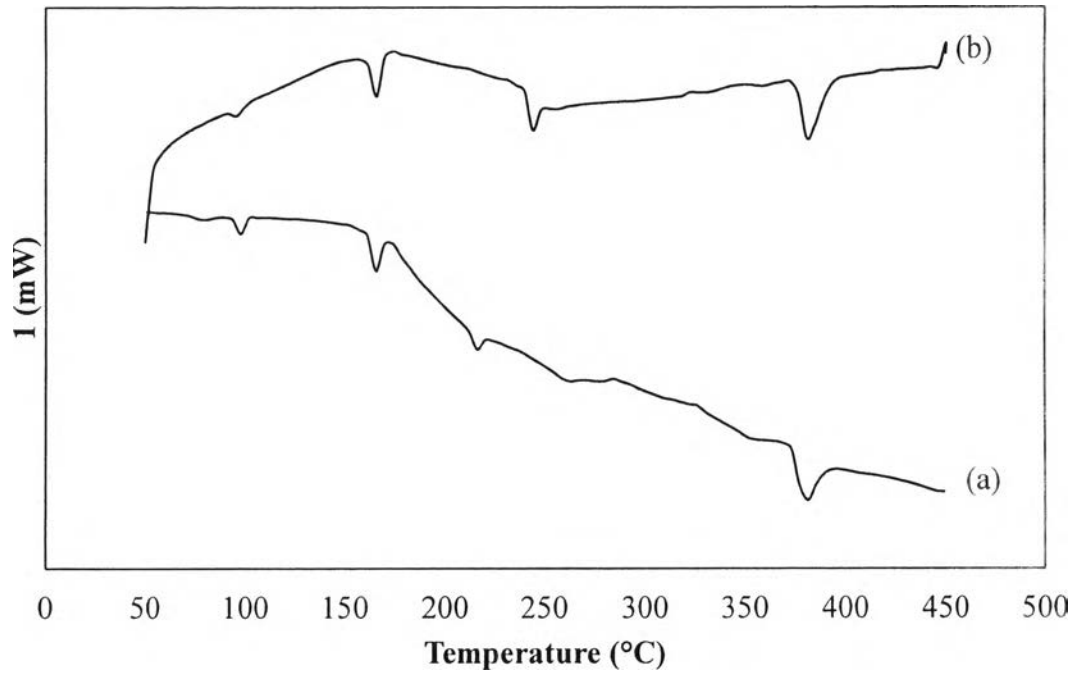

Figure 4.4 Differential scanning calorimetry profiles of the $LiBH_4/MgCl_2$ mixture milled for 2 h (a) and 5 h (b).

The results from Figures 4.3 and 4.4 exhibit that using different ball milling times results in similar hydrogen desorption behavior and desorption temperature. However, the $LiBH_4/MgCl_2$ mixture milled for 2 h shows a little higher hydrogen capacity than that milled for 5 h. Moreover, for the dehydrogenation rate, the $LiBH_4/MgCl_2$ mixture milled for 2 h also shows a higher desorption rate. It can be seen that the initial hydrogen desorption of the $LiBH_4/MgCl_2$ mixture milled for 2 h is higher than the mixture milled for 5 h (Figure 4.5).

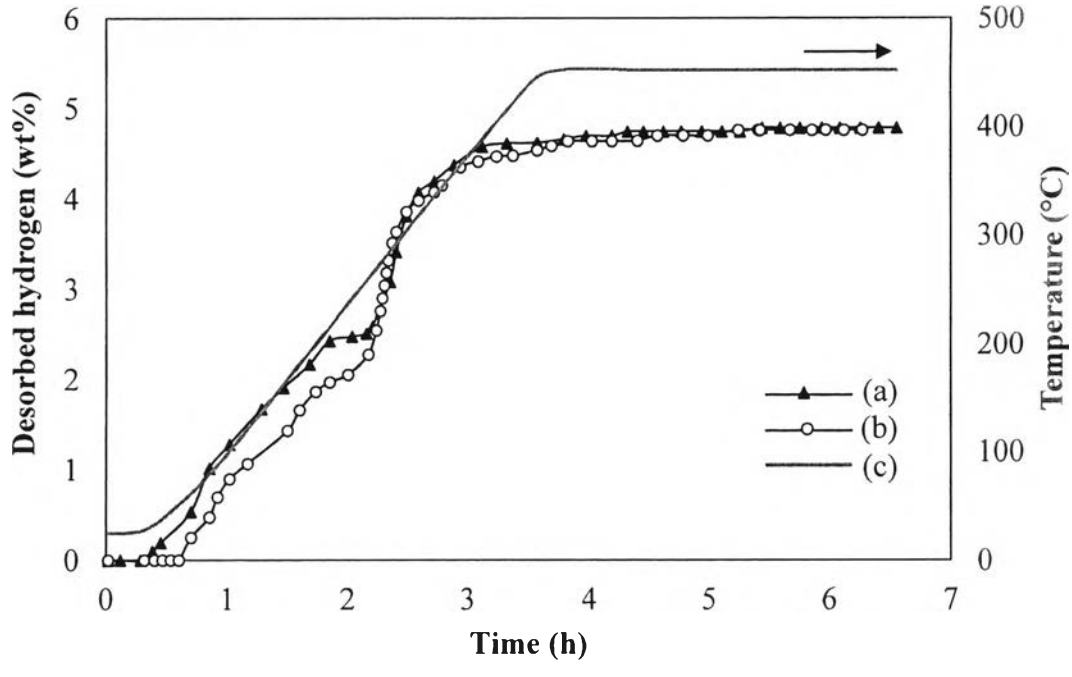

Figure 4.5 Hydrogen desorption profiles as a function of time of the $LiBH_4/MgCl_2$ mixture after ball milling for 2 h (a), 5 h (b), and (c) temperature.

4.2 Hydrogen Desorption of Catalyzed $Mg(BH_4)_2$

4.2.1 Effects of TiO_2 and Nb_2O_5

It is well known that catalysts are an important factor that affects the desorption temperature of metal hydrides and complex metal hydrides (Sakintuna *et al.*, 2007). There are many types of catalysts, each of which provides different effects on the hydrogen desorption properties of the hydride. This work further substantiates the effects of a catalyst on the desorption behaviors of $Mg(BH_4)_2$ with 16 wt% of TiO_2 and Nb_2O_5.

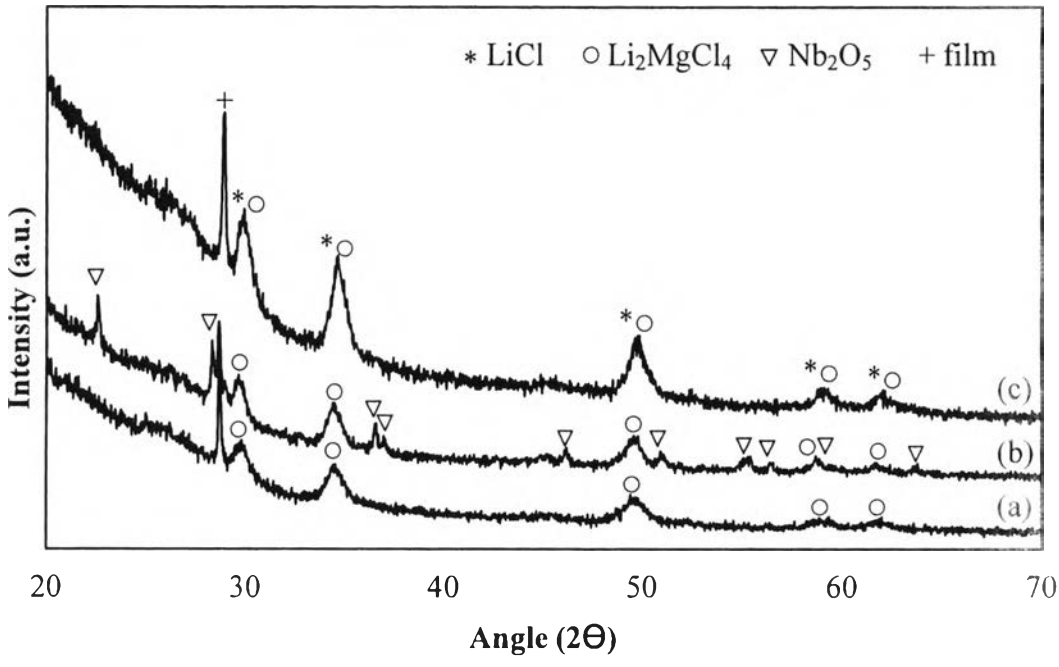

Figure 4.6 X-ray diffraction patterns of 16 wt% TiO_2-$LiBH_4/MgCl_2$ (a) and16 wt% Nb_2O_5-$LiBH_4/MgCl_2$ (b) milled for 2 h and X-ray diffraction patterns of the $LiBH_4/MgCl_2$ mixture milled for 2 h (c).

The XRD patterns of the mixture after ball milling are shown in Figure 4.6. It can be seen that the peak intensities of all doped samples (Figure 4.6(a) and 4.6(b)) are weaker and boarder than the undoped one (Figure 4.6(c)), this implies that Nb_2O_5 and TiO_2 can reduce the crystallite size (Sridechprasat, 2011). For TiO_2-$LiBH_4/MgCl_2$ (Figure 4.6(a)), the peak of TiO_2 is absence that may be resulted from the crystallized structure of TiO_2 is destroyed during the ball milling process. In addition, the XRD patterns after ball milling reveal that the undoped sample (Figure 4.6(c)) and the sample doped with Nb_2O_5 (Figure 4.6(a)) and TiO_2 (Figure 4.6(b)) form the Li_2MgCl_4 phase, which is an intermediate compound from the reaction between $LiBH_4$ and $MgCl_2$.

TiO_2 is one of the titanium catalysts that can improve the performance of metal hydride, and Figure 4.7 shows the hydrogen desorption profiles of 16 wt% TiO_2-$LiBH_4/MgCl_2$ with 2 and 5 h ball milling times. Hydrogen desorbs in two steps same as the uncatalyzed sample. 16 wt% TiO_2-$LiBH_4/MgCl_2$ ball milled for 2 h (Figure 4.7(a)) starts to decompose at 41 °C, and the first desorption step occurs at

246 °C and releases about 3.25 wt% hydrogen. The second step releases 1.74 wt% hydrogen at 303 °C with the total hydrogen of 5.27 wt%. 16 wt% TiO_2-$LiBH_4/MgCl_2$ ball milled for 5 h (Figure 4.7(b)) shows similar hydrogen desorption profile to the one ball milled for 2 h. It starts to desorb at 41°C and the first desorption step appear at 249 °C with 3.10 wt% hydrogen. The second step releases 1.75 wt% hydrogen at 307 °C and provides the total hydrogen capacity of 5.03 wt%. The results indicate that TiO_2 improves the desorption behaviors of $Mg(BH_4)_2$ that is to decrease the desorption temperature at the second step about 71 °C and 67 °C for the samples ball milled for 2 h and 5 h, respectively.

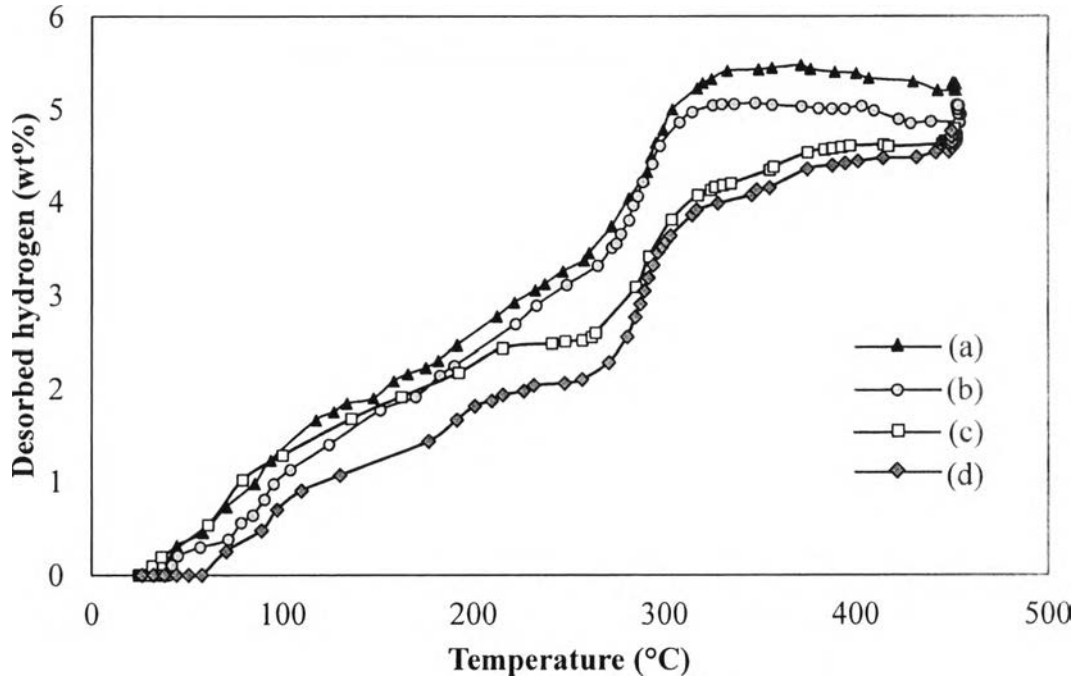

Figure 4.7 Hydrogen desorption profiles of 16wt% TiO_2-$LiBH_4/MgCl_2$ milled for 2 h (a) and 5 h (b) and hydrogen desorption profiles of the $LiBH_4/MgCl_2$ mixture milled for 2 h (c) and 5 h (d).

For the desorption rate, it can be seen that TiO_2 doped samples show a higher amount of hydrogen than the undoped samples (Figure 4.8). In addition, 16wt% TiO_2-$LiBH_4/MgCl_2$ milled for 2 h shows higher initial desorption rate than 5 h according to the hydrogen desorption profiles as a function of time (Figure 4.8(a)

and 4.8(b)). This result also supports that the ball milling time for 2 h is sufficient to prepare $Mg(BH_4)_2$ and doped-$Mg(BH_4)_2$.

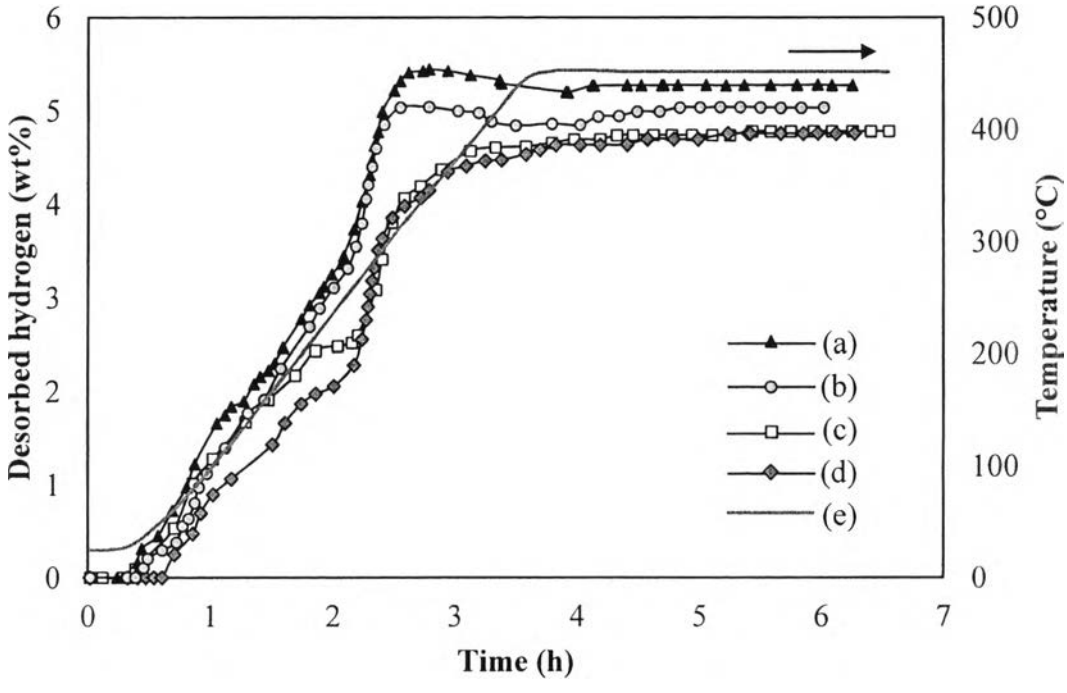

Figure 4.8 Hydrogen desorption profiles as a function of time of 16wt% TiO_2-$LiBH_4/MgCl_2$ milled for 2 h (a) and 5 h (b) and hydrogen desorption profiles of the $LiBH_4/MgCl_2$ mixture milled for 2 h (c) and 5 h (d) and temperature (e).

The hydrogen desorption profiles of 16 wt% Nb_2O_5-$LiBH_4/MgCl_2$ with 2 and 5 h ball milling times are presented in Figure 4.9. The samples release hydrogen in two steps as the uncatalyzed sample. For 16 wt% Nb_2O_5-$LiBH_4/MgCl_2$ ball milled for 2 h (Figure 4.9(a)), it starts to decompose at 31 °C. The first step desorption releases 3.20 wt% hydrogen and takes place at 236 °C, while the start of the second desorption is at 308 °C with 1.40 wt% hydrogen, and the total amount of desorbed hydrogen is about 4.86 wt%. 16 wt% Nb_2O_5-$LiBH_4/MgCl_2$ ball milled for 5 h (Figure 4.9(b)) shows the first desorption step at 241 °C and releases 2.79 wt% hydrogen, whereas the second step occurs at 307 °C with 1.49 wt% hydrogen and the total desorbed hydrogen of 4.73 wt%. The results suggest that Nb_2O_5 improves the desorption behaviors of $Mg(BH_4)_2$, which is to decrease the desorption temperature at the second step from 374 °C (uncatalyzed) to 308 °C and

307 °C for 16 wt% Nb_2O_5-$LiBH_4/MgCl_2$ ball milled for 2 and 5 h, respectively. These result also supports that the ball milling time of 2 h is sufficient to prepare $Mg(BH_4)_2$ with the used amounts of Nb_2O_5. Therefore, the addition of Nb_2O_5 contributes to fast hydrogen desorption with a significant decrease of desorption temperature about 65 °C, which is in agreement with that reported by Friedrichs *et al.* (2006).

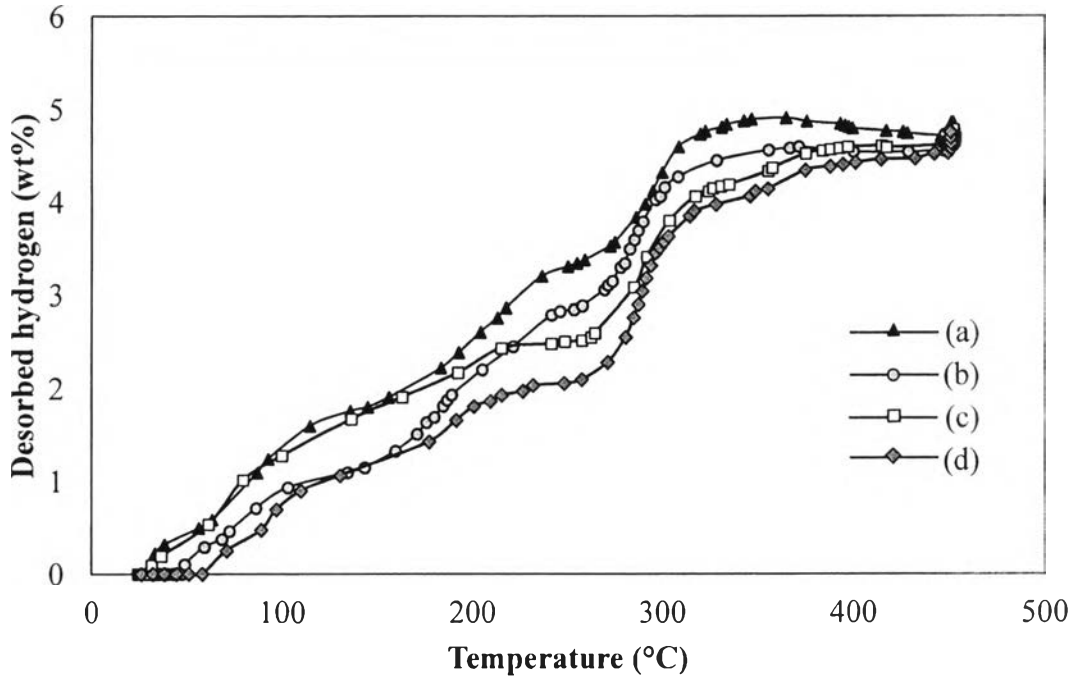

Figure 4.9 Hydrogen desorption profiles of 16wt% Nb_2O_5- $LiBH_4/MgCl_2$ milled for 2 h (a) and 5 h (b) and hydrogen desorption profiles of the $LiBH_4/MgCl_2$ mixture milled for 2 h (c) and 5 h (d).

For the dehydrogenation rate, 16 wt% Nb_2O_5-$LiBH_4/MgCl_2$ milled for 2 h also shows a higher desorption rate than 5 h (Figure 4.10(a) and 4.10(b)). It can be seen that the desorption kinetics at the initial period of 16 wt% Nb_2O_5-$LiBH_4/MgCl_2$ ball milling for 2 h is higher than 5 h. Moreover, samples doped with Nb_2O_5 increase the desorption kinetics of both undoped samples, 2 and 5 h (Figure 4.10).

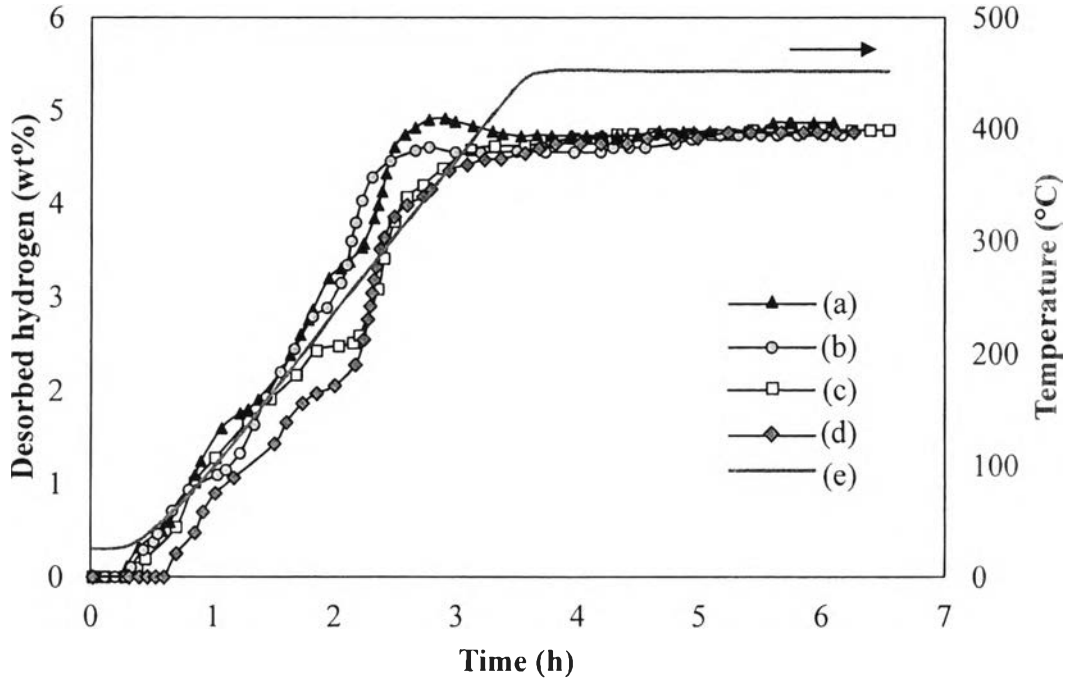

Figure 4.10 Hydrogen desorption profiles as a function of time of 16wt% Nb_2O_5-$LiBH_4/MgCl_2$ milled for 2 h (a) and 5 h (b) and hydrogen desorption profiles of the $LiBH_4/MgCl_2$ mixture milled for 2 h (c) and 5 h (d) and temperature (e).

The comparison of hydrogen desorption profiles between the undoped, Nb_2O_5, and TiO_2 doped samples milled for 2 h are shown in Figures 4.11 4.12. It can be seen from the figures that TiO_2 doped samples show the best behavior, which not only decreases the desorption temperature but also improves the hydrogen desorption capacity.

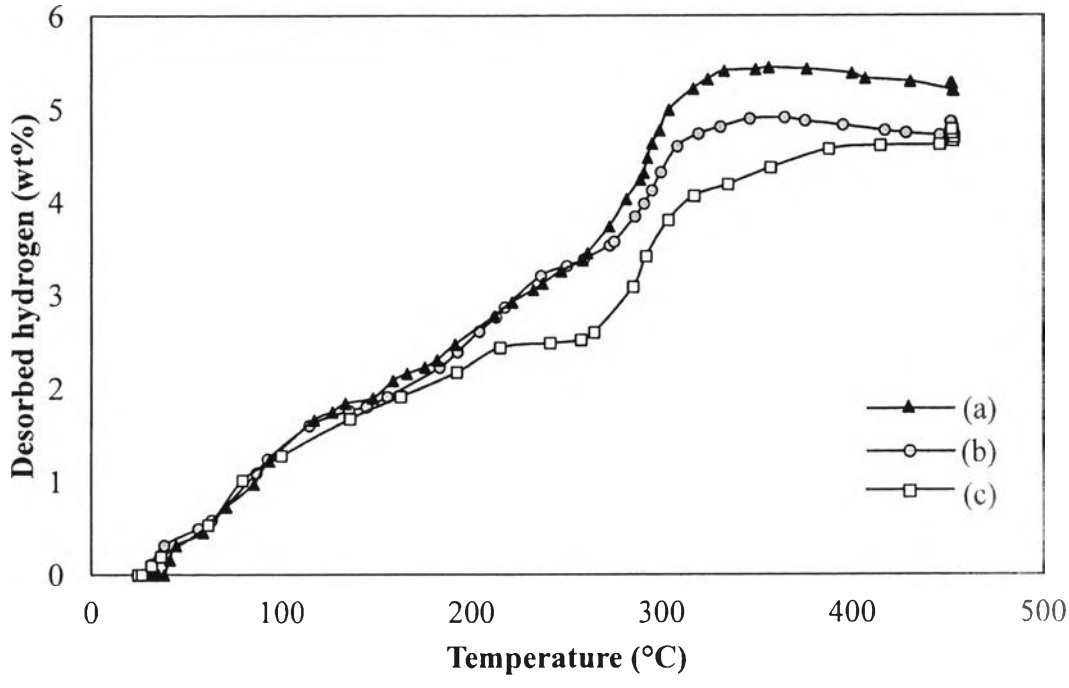

Figure 4.11 Hydrogen desorption profiles of 16wt% TiO_2-$LiBH_4$/$MgCl_2$ (a), and 16 wt% Nb_2O_5-$LiBH_4$/$MgCl_2$ milled for 2 (b) and hydrogen desorption profiles of the $LiBH_4$/$MgCl_2$ mixture milled for 2 h (c).

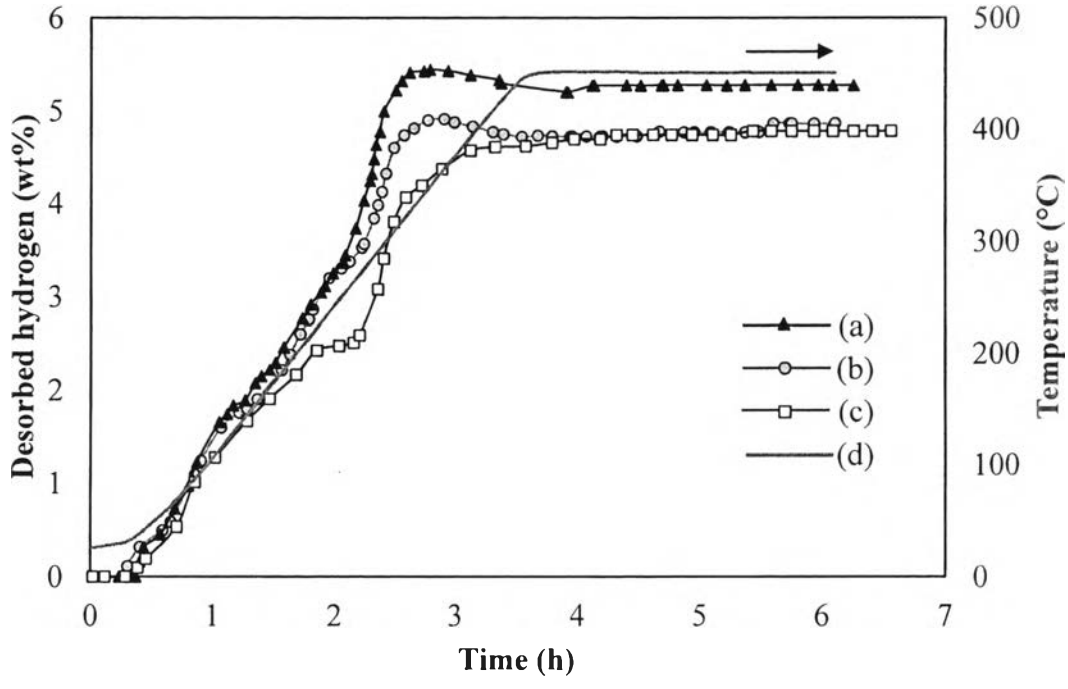

Figure 4.12 Hydrogen desorption profiles as a function of time of 16wt% TiO_2-$LiBH_4/MgCl_2$ (a), and 16 wt% Nb_2O_5-$LiBH_4/MgCl_2$ milled for 2 (b) and hydrogen desorption profiles of the $LiBH_4/MgCl_2$ mixture milled for 2 h (c) and temperature (d).

From Table 4.1, the undoped, Nb_2O_5, and TiO_2 doped samples ball milled for 2 h desorb 4.78, 4.86, and 5.27 wt% hydrogen, respectively. The undoped, Nb_2O_5, and TiO_2 doped samples ball milled for 5 h desorb 4.76, 4.73, and 5.03 wt% hydrogen, respectively. From these results, it was found that the sample with 16 wt% TiO_2 releases higher amounts of hydrogen than the undoped and 16 wt% Nb_2O_5 doped samples and also decreases the hydrogen desorption temperature of the hydride in the second step decomposition. According to a study by Jung *et al.* (2007), the use of nanosized rutile TiO_2 in MgH_2 creates a greater reactive surface with hydrogen, and the capacity was increased by forming an ultra-fine nanocomposite of MgH_2-rutile TiO_2. Furthermore, the reduction of the Ti^{4+} ions in TiO_2 to metallic Ti^0 appears to result in the formation of active species responsible for catalyzing the MgH_2 dehydrogenation reaction (Croston *et al.*, 2010).

Table 4.1 Hydrogen desorption temperature and total amount of desorption hydrogen of the $LiBH_4/MgCl_2$ mixture and the mixture doped with different catalysts (16 wt% Nb_2O_5 and 16 wt%TiO_2) after ball milling for 2 and 5 h

$LiBH_4/MgCl_2$ mixture	Desorption temperature, °C			Hydrogen capacity, wt%		
	Undoped	Nb_2O_5	TiO_2	Undoped	Nb_2O_5	TiO_2
Ball milled 2h						
Step 1	214	236	246	2.43	3.20	3.25
Step 2	374	308	303	2.10	1.40	1.74
Total H_2 (wt %)				4.78	4.86	5.27
Ball milled5 h						
Step 1	226	241	249	1.97	2.79	3.10
Step 2	374	307	307	2.56	1.49	1.75
Total H_2 (wt %)				4.76	4.73	5.03

The XRD patterns of the mixture after the hydrogen desorption at 450 °C are shown in Figure 4.13. The XRD patterns after desorption are similar to the one obtained after ball milling, which is in agreement with that reported by Varin and Zbroniec (2010), who reported the hydrogen desorption from the $LiBH_4/MnCl_2$ mixture. However, it can be seen from the figure that all samples have the same phase of LiCl, and the Li_2MgCl_4 phase that appear in the XRD patterns after ball milling disappears after the desorption process. The absence of Li_2MgCl_4 indicates that heat from the desorption process may decompose this compound resulting in the LiCl phase. The presence of $LiCl(H_2O)$ and LiO phases (Figure 4.13(c)) may be from impurities and moisture during the sample preparation. From Figure 4.13(b), the presence of NbO is resulted from the reduction of Nb_2O_5 during the desorption process. NbO is believed to improve the dehydrogenation kinetics of $Mg(BH_4)_2$ by a formation pathways of niobium oxide species with lower oxidation state, which facilitates the hydrogen transport from the sample (Fan *et al.*, 2008). For the XRD

pattern of 16 wt% TiO_2-$LiBH_4$/$MgCl_2$ (Figure 4.13(a)), the peak of Ti is not present as it may be in the amorphous form.

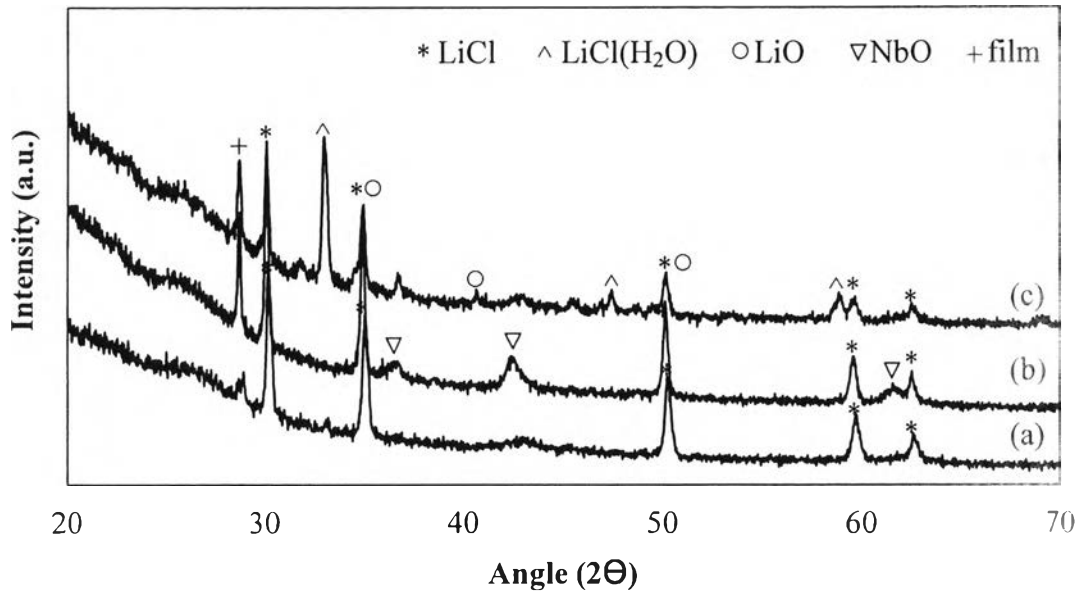

Figure 4.13 X-ray diffraction patterns of the 16 wt% TiO_2-$LiBH_4$/$MgCl_2$ (a) and 16 wt% Nb_2O_5-$LiBH_4$/$MgCl_2$ (b) after the hydrogen desorption at 450 °C and X-ray diffraction patterns of the $LiBH_4$/$MgCl_2$ mixture after the hydrogen desorption (c).

4.2.2 Effects of Ti-based Catalysts

The desorption behavior of 16 wt% TiO_2-$LiBH_4$/$MgCl_2$ ball milled for 2 h shows that the additive TiO_2 not only decreases the desorption temperature but also results in the high desorption capacity. Therefore, other Ti-based catalysts are potential candidates to reduce the onset temperatures of dehydrogenation and increase hydrogenation and dehydrogenation rates. This part of study is to investigate the effects of Ti and $TiCl_3$ catalysts including TiO_2 catalyst on the hydrogen desorption of $LiBH_4$/$MgCl_2$.

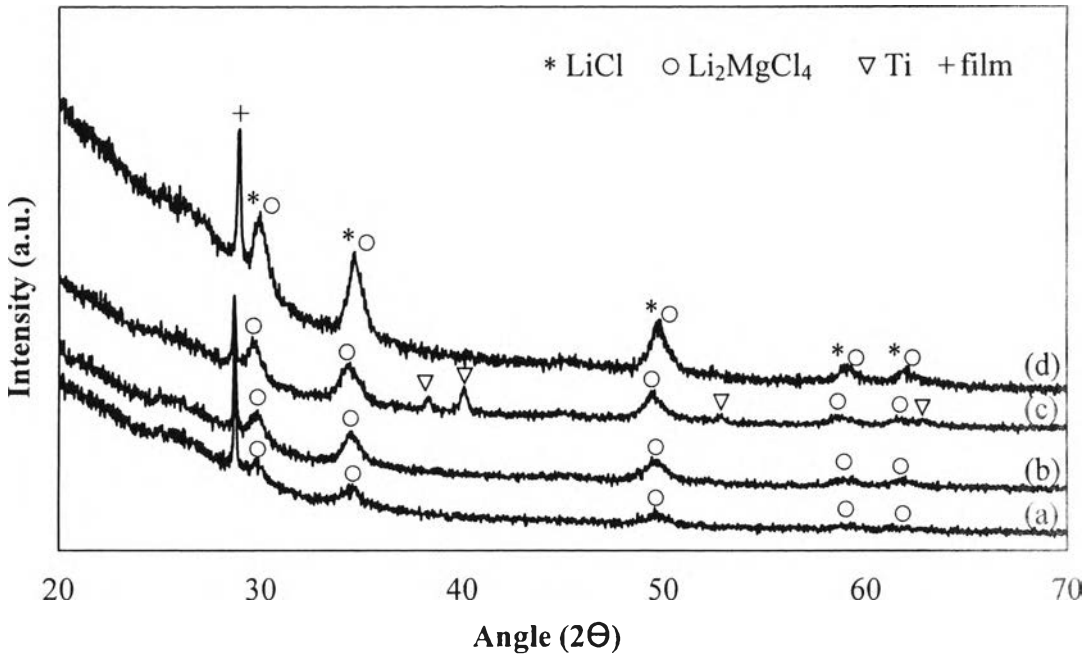

Figure 4.14 X-ray diffraction patterns of 16 wt% $TiCl_3$-$LiBH_4/MgCl_2$ (a), 16 wt% TiO_2-$LiBH_4/MgCl_2$ (b), and 16 wt% Ti-$LiBH_4/MgCl_2$ (c) milled for 2 h and X-ray diffraction patterns of the $LiBH_4/MgCl_2$ mixture milled for 2 h (d).

According to the XRD patterns of the $LiBH_4/MgCl_2$ mixture and all doped samples with the Ti-based catalysts after ball-milling for 2 h (Figure 4.14), they show the same Li_2MgCl_4 peak, which is an intermediate compound from the reaction between $LiBH_4$ and $MgCl_2$. It can be seen that the peak intensities of all doped samples (Figure 4.14(a)-(c)) are boarder than the undoped one (Figure 4.14(a)). This implies that the titanium catalysts can reduce the crystallize size of the $LiBH_4/MgCl_2$ mixture. Figure 4.14(c) shows the Ti phase corresponding to the addition of 16 wt% Ti. A possible reason may be because among the doped samples, the one with Ti has the largest crystallite size and the hardness of Ti particles, which is higher than that of TiO_2 and $TiCl_3$ particles (Sridechprasat, 2011).

Hydrogen desorption profiles of the $LiBH_4/MgCl_2$ mixture and the mixture doped with 16 wt% of Ti, TiO_2, and $TiCl_3$ are shown in Figure 4.15.

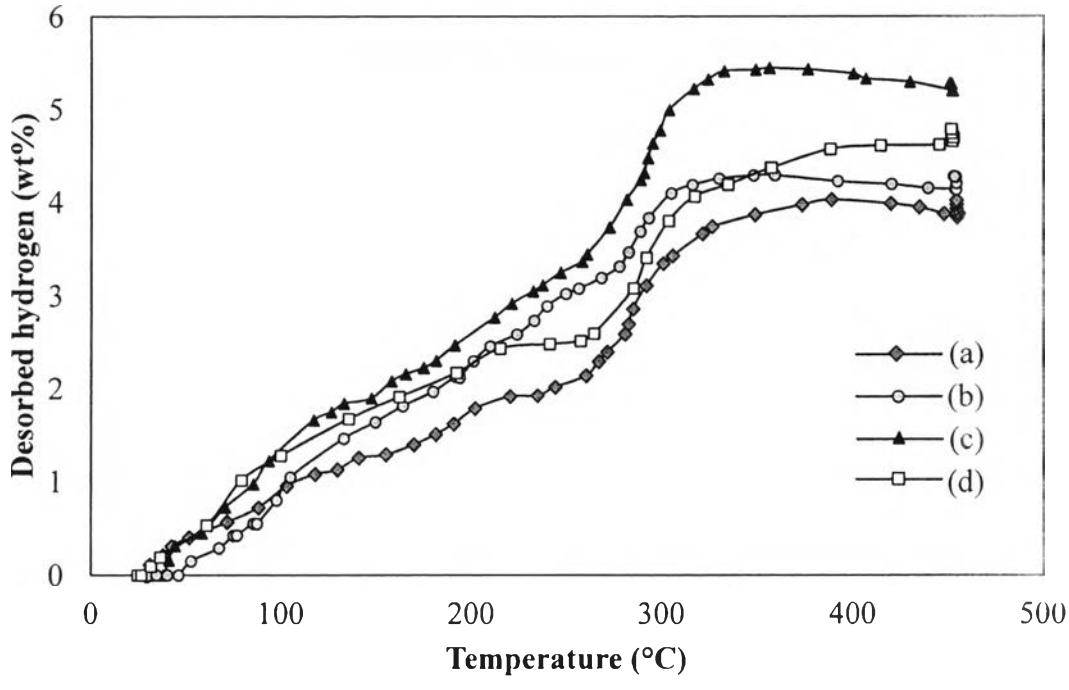

Figure 4.15 Hydrogen desorption profiles of 16wt% Ti-$LiBH_4/MgCl_2$ (a), $TiCl_3$-$LiBH_4/MgCl_2$ (b), and TiO_2-$LiBH_4/MgCl_2$ (c) milled for 2 h and hydrogen desorption profiles of the $LiBH_4/MgCl_2$ mixture milled for 2 h (d).

In the desorption process, the $LiBH_4/MgCl_2$ (Figure 4.15(d)), 16 wt% Ti-$LiBH_4/MgCl_2$ (Figure 4.15(a)), 16 wt% $TiCl_3$-$LiBH_4/MgCl_2$ (Figure 4.15(b)), and 16 wt% TiO_2-$LiBH_4/MgCl_2$ (Figure 4.15(c)) mixtures milled for 2 h decompose in two steps with different desorption temperatures. For the desorption temperature, all doped samples start to release hydrogen at a little higher temperature than the undoped sample. For the amount of desorbed hydrogen, it was found that, with TiO_2, the sample releases the highest amount of hydrogen whereas Ti and $TiCl_3$ doped samples release lower amounts of hydrogen than the undoped sample. From Table 4.2, the amount of desorbed hydrogen in the first step is 2.43 wt% for the undoped sample, 1.91 wt% for the Ti doped sample, 3.03 wt% for $TiCl_3$ doped sample, and 3.25 wt% for TiO_2 doped sample. The catalytic activity of $TiCl_3$ and TiO_2 shows similar effects on the $LiBH_4/MgCl_2$ mixture as that on the $LiBH_4$ and MgH_2 mixture (Sridechprasat, 2011). In the case of Ti, the XRD pattern after ball

milling process still shows the peak of Ti phase that may not interact with the $LiBH_4/MgCl_2$ mixture resulting in the lower amount of hydrogen desorption and does not affect the desorption temperature. Regarding the fast hydrogen sorption kinetics of nanocrystalline Mg using metal oxide as catalyst. Barkhordarian *et al.* (2003) showed that oxides and chlorides of metals with multiple valence states have larger catalytic effects than the metal catalyst.

16 wt% Ti-$LiBH_4/MgCl_2$ ball milled for 2 h (Figure 4.15(a)) starts to decompose at 31 °C, and the first desorption step occurs at 272 °C and releases about 1.92 wt% hydrogen. For $TiCl_3$, it starts to desorb at 52°C and the first desorption step appears at 249 °C with 3.02 wt% hydrogen (Figure 4.15(b)). Doping $TiCl_3$ and TiO_2 catalysts decrease the hydrogen desorption temperature of the hydride in the second step decomposition about 70 °C. The doped $TiCl_3$ and TiO_2 samples liberate hydrogen in this step at 304 °C and 303 °C, respectively (Figure 4.15(b) and 4.15(c)), which is lower than that doped with Ti and the undoped one, 372 °C and 374 °C, respectively. It can be seen that $TiCl_3$ and TiO_2 catalysts play an important role in the reduction of the hydrogen desorption temperature. However, the cumulative amounts of desorbed hydrogen in this step of Ti, and $TiCl_3$ doped samples are lower than the undoped one. The Ti and $TiCl_3$ doped samples desorb 2.06, and 1.08 wt% hydrogen, respectively, while the undoped sample releases 2.56 wt% hydrogen (Table 4.2). These results were similar to the report of Suttisawat *et al.* (2010) that TiO_2 catalyst showed better re-absorption rate than $TiCl_3$ catalyst. This is due to the surface area of the desorbed sample of TiO_2-$NaAlH_4$ is higher than $TiCl_3$-$NaAlH_4$, which indicates that TiO_2 facilitates the hydrogen diffusion in the desorbed sample because its porosity and surface area increase the surface area of the hydride sample. Furthermore, the one doped with Ti catalyst gives the lowest total amount of desorbed hydrogen (4.02 wt%). A possible reason may be because the Ti^0 defect sites may further form a microstructure composite with the host metal lattice framework and/or transform to the titanium hydride phase of $TiH_{x<2}$ that may inhibit the activity of Ti catalyst resulting in the lower amount of hydrogen desorption (Sridechprasat, 2011).

Hydrogen desorption profiles as a function of time of the Ti-based catalyst are shown in Figure 4.14. It can be seen that the sample doped with $TiCl_3$

and TiO_2 (Figure 4.16(b)-(c)) show faster hydrogen desorption rate than the sample doped with Ti (Figure 4.16(a)) and the undoped one (Figure 4.16(d)).

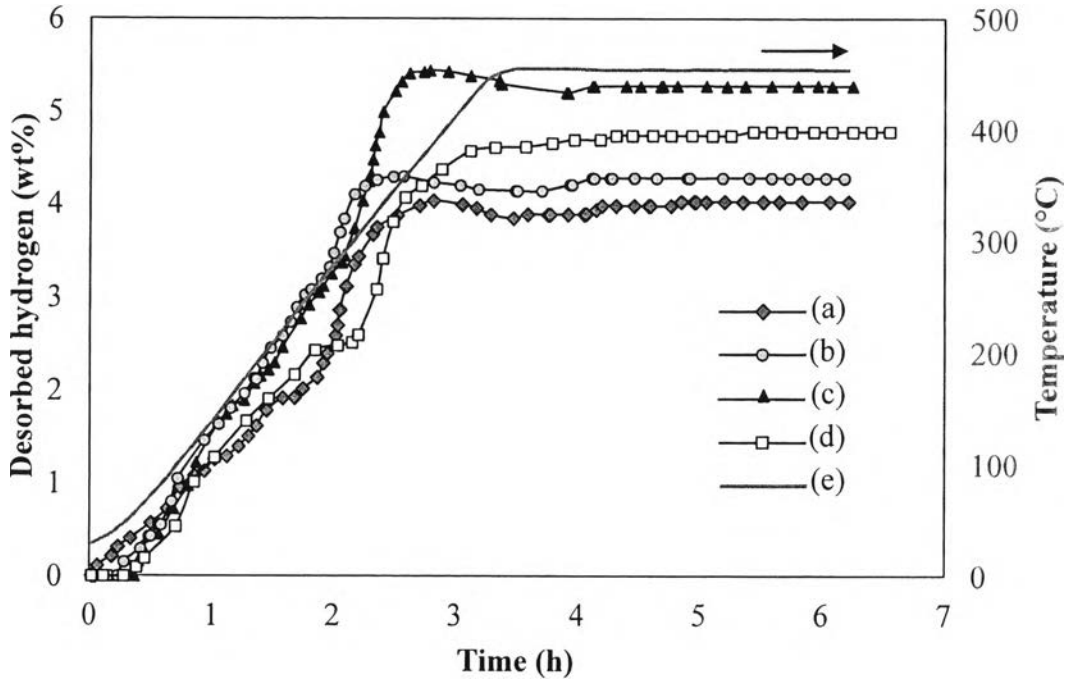

Figure 4.16 Hydrogen desorption profiles as a function of time of 16wt% Ti-$LiBH_4/MgCl_2$ (a), $TiCl_3$- $LiBH_4/MgCl_2$ (b), and TiO_2- $LiBH_4/MgCl_2$ (c) milled for 2 h and hydrogen desorption profiles of the $LiBH_4/MgCl_2$ mixture milled for 2 h (d) and temperature (e).

For the total amount of desorbed hydrogen, the doped samples release lower amounts of hydrogen than the undoped one except TiO_2. From Table 4.2, the undoped, Ti, TiO_2 and $TiCl_3$ doped samples desorb 4.78, 4.02, 5.27, and 4.27 wt% hydrogen, respectively. It can be deduced that using TiO_2 not only results in the low desorption temperature but also high hydrogen capacity, while using Ti does not affect the desorption temperature of on the $LiBH_4/MgCl_2$ mixture.

Table 4.2 Hydrogen desorption temperature and total amount of desorption hydrogen of the $LiBH_4/MgCl_2$ mixture and the mixture doped with different titanium catalysts after ball milling for 2 h

$LiBH_4/MgCl_2$ mixture	Desorption temperature, °C				Hydrogen capacity, wt%			
	Undoped	Ti	$TiCl_3$	TiO_2	Undoped	Ti	$TiCl_3$	TiO_2
Step 1	214	234	249	246	2.43	1.92	3.02	3.25
Step 2	374	372	304	303	2.10	2.06	1.08	1.74
Total H_2 (wt%)					4.78	4.02	4.27	5.27

The XRD patterns of the mixtures after the hydrogen desorption at 450 °C are shown in Figure 4.17. The XRD patterns after the desorption are similar to the one obtained after ball milling (Figure 4.14), and all samples have the same phase of LiCl whereas the Li_2MgCl_4 phase that appear in the XRD patterns after ball milling disappears after the desorption process. In addition, the XRD patterns of 16 wt% $TiCl_3$-$LiBH_4/MgCl_2$ (Figure 4.17(a)) show the phase of MgO, which is an oxide layer from the reaction between Mg and impurities (Sridechprasat, 2011). The Ti phase, which is in the Ti doped sample after ball milling (Figure 4.14(c)), is also in the sample after hydrogen desorption process (Figure 4.17(c)) indicating that some part of Ti catalyst does not interact with the $LiBH_4/MgCl_2$ mixture. Therefore, this result supports that Ti does not show any effect on the desorption temperature and the hydrogen capacity whereas the other catalysts can decrease the desorption temperature at the second step.

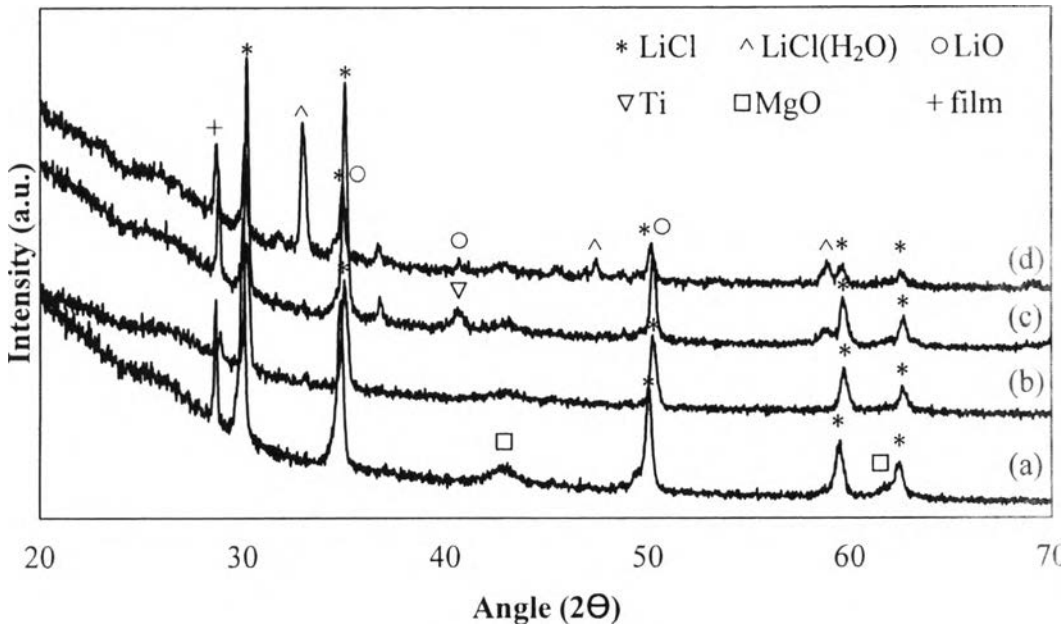

Figure 4.17 X-ray diffraction patterns of 16 wt% $TiCl_3$-$LiBH_4/MgCl_2$ (a), 16 wt% TiO_2-$LiBH_4/MgCl_2$ (b), and 16 wt% Ti-$LiBH_4/MgCl_2$ (c) and X-ray diffraction patterns of the $LiBH_4/MgCl_2$ mixture after the hydrogen desorption (d).

4.2.3 Effect of Nb-based Catalysts

It is well known that transition metal chlorides and metal oxides show catalytic activity for complex hydrides (Bardají *et al.*, 2011). Kim *et al.* (2008) reported the effects of Nb-catalysts (NbF_5 and $NbCl_5$) on the reversibility of $Ca(BH_4)_2$ that the Nb-catalysts decrease the hydrogen desorption temperature. Moreover, the desorption profile of 16 wt% Nb_2O_5-$LiBH_4/MgCl_2$ ball milled for 2 h shows the lower desorption temperature than the undoped one at the second step. Therefore, effects of Nb-based catalysts on the hydrogen desorption temperature and the desorption kinetics to the $LiBH_4/MgCl_2$ mixture was investigated.

The XRD patterns of the mixtures after ball milling are shown in Figure 4.18. It can be seen that the peak intensities of all doped samples (Figure 4.18(a) and 4.18(b)) are weaker and boarder than the undoped one (Figure 4.18(c)) similar to the XRD patterns of that doped with the Ti-based catalysts (Figure 4.14). For $NbCl_5$-$LiBH_4/MgCl_2$ (Figure 4.18(a)), the peak of $NbCl_5$ is absence that may be due to the crystallized structure of $NbCl_5$ is destroyed during the ball milling process.

Nb_2O_5-$LiBH_4$/$MgCl_2$ shows the peak of Nb_2O_5, which indicates that ball milling process does not destroy the crystalline structure of Nb_2O_5. In addition, the Li_2MgCl_4 peak is shown in all samples.

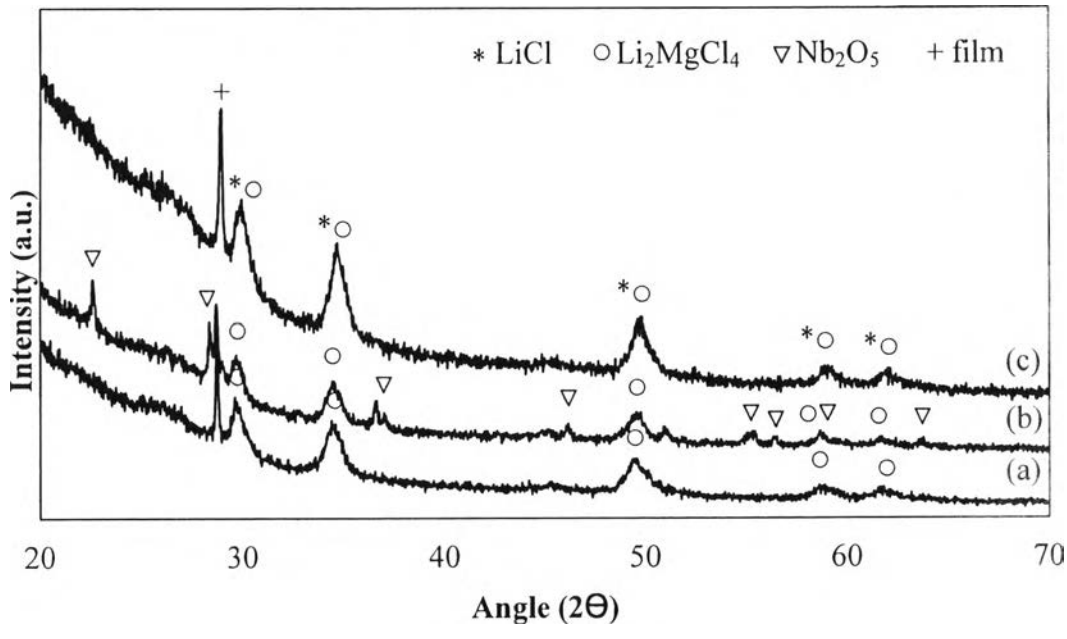

Figure 4.18 X-ray diffraction patterns of 16 wt% $NbCl_5$-$LiBH_4$/$MgCl_2$ (a) and 16 wt% Nb_2O_5-$LiBH_4$/$MgCl_2$ (b) milled for 2 h and X-ray diffraction patterns of the $LiBH_4$/$MgCl_2$ mixture milled for 2 h (c).

Hydrogen desorption profiles of the $LiBH_4$/$MgCl_2$ mixture and the mixture doped with 16 wt% of $NbCl_5$, and Nb_2O_5 are shown in Figure 4.19. 16 wt% of $NbCl_5$-$LiBH_4$/$MgCl_2$ starts to desorb hydrogen at 48 °C, which is a little higher than the starting desorption temperature of 16 wt% Nb_2O_5-$LiBH_4$/$MgCl_2$ and undoped sample. It can be seen that the hydrogen desorption profile of $NbCl_5$ doped sample (Figure 4.19(b)) does not clearly show curve of the first desorption step, whereas the second desorption step occurs at 329 °C. However, both doped samples exhibit the hydrogen desorption of the second step at the lower temperature than that of the undoped one. $NbCl_5$ and Nb_2O_5 catalysts can decrease the desorption temperature at the second desorption step about 40 °C and 70 °C, respectively.

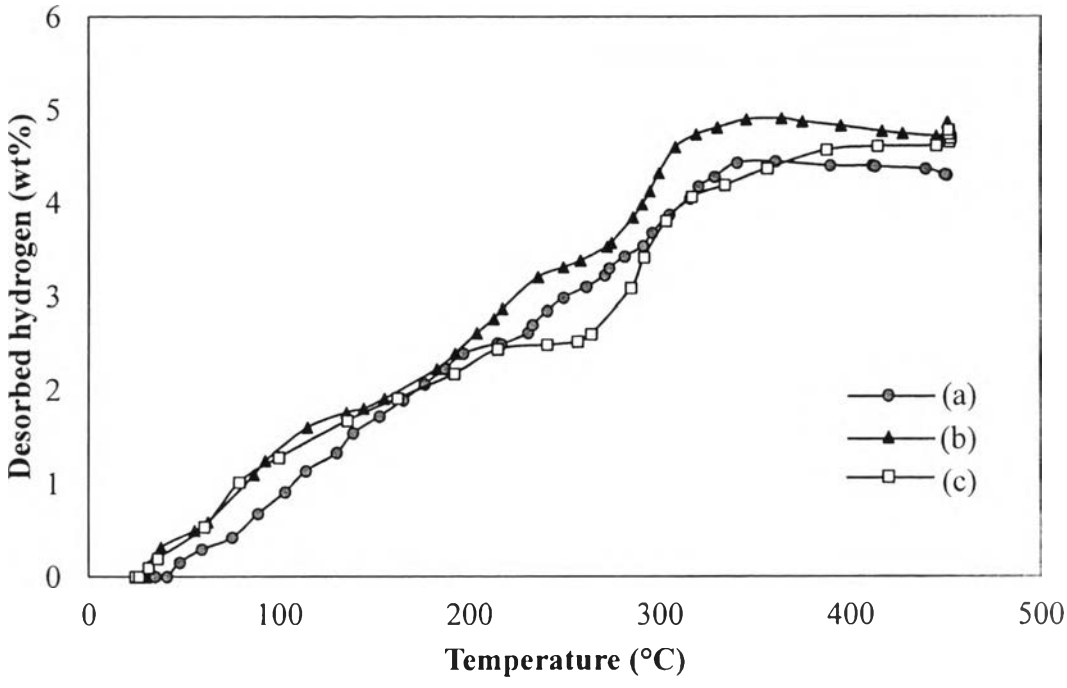

Figure 4.19 Hydrogen desorption profiles of 16 wt% $NbCl_5$-$LiBH_4/MgCl_2$ mixture (a), and 16 wt% Nb_2O_5-$LiBH_4/MgCl_2$ mixture (b) milled for 2 h and hydrogen desorption profiles of the $LiBH_4/MgCl_2$ mixture milled for 2 h (c).

The hydrogen desorption of Nb-based catalysts as a function of time are shown in Figure 4.20. Both doped samples (Figure 4.20(a)-(b)) show higher desorption rate than the undoped one (Figure 4.20(c)) at the first and second step of the decomposition. However, 16 wt% $NbCl_5$-$LiBH_4/MgCl_2$ has a lower hydrogen capacity than the undoped sample whereas 16 wt% Nb_2O_5-$LiBH_4/MgCl_2$ shows the hydrogen capacity close to the undoped sample. From Table 4.3, the undoped, $NbCl_5$, and Nb_2O_5 doped samples desorb 4.78, 4.86, and 4.30 wt% hydrogen, respectively.

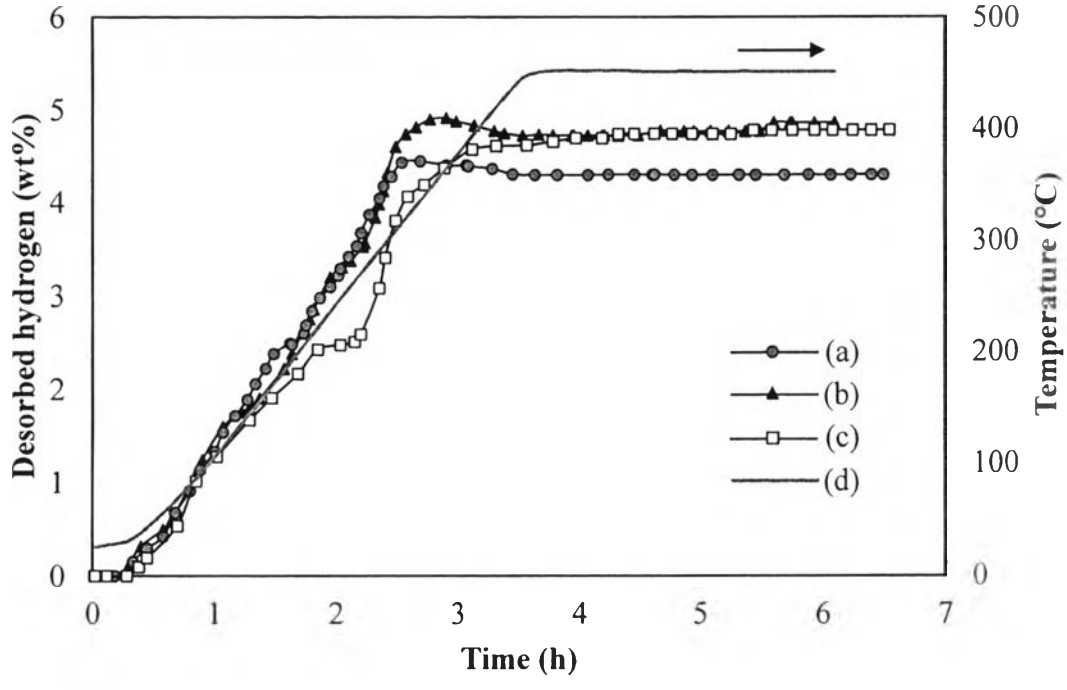

Figure 4.20 Hydrogen desorption profiles as a function of time of 16wt% $NbCl_5$-$LiBH_4/MgCl_2$ (a), and Nb_2O_5-$LiBH_4/MgCl_2$ (b) milled for 2 h and hydrogen desorption profiles of the $LiBH_4/MgCl_2$ mixture milled for 2 h (c) and temperature (d).

Table 4.3 Hydrogen desorption temperature and total amount of desorption hydrogen of the $LiBH_4/MgCl_2$ mixture and the mixture doped with different niobium catalysts after ball milling for 2 h

$LiBH_4/MgCl_2$ mixture	Desorption temperature, °C			Hydrogen capacity, wt%		
	Undoped	Nb_2O_5	$NbCl_5$	Undoped	Nb_2O_5	$NbCl_5$
Step 1	214	236	231	2.43	3.20	2.60
Step 2	374	308	329	2.10	1.40	1.59
Total H_2 (wt %)				4.78	4.86	4.30

The phase identification of the samples after the hydrogen desorption is shown in Figure 4.21. It can be seen from that all samples have the same dominant phase of LiCl. The unclear desorption profile of 16wt% $NbCl_5$-$LiBH_4/MgCl_2$ may be from the excess Cl element. The MgO phase (Figure 4.21(a)) is the oxide layer from the reaction between Mg and impurities similar to the XRD result of 16 wt% $TiCl_3$-$LiBH_4/MgCl_2$ (Figure 4.17(a)).

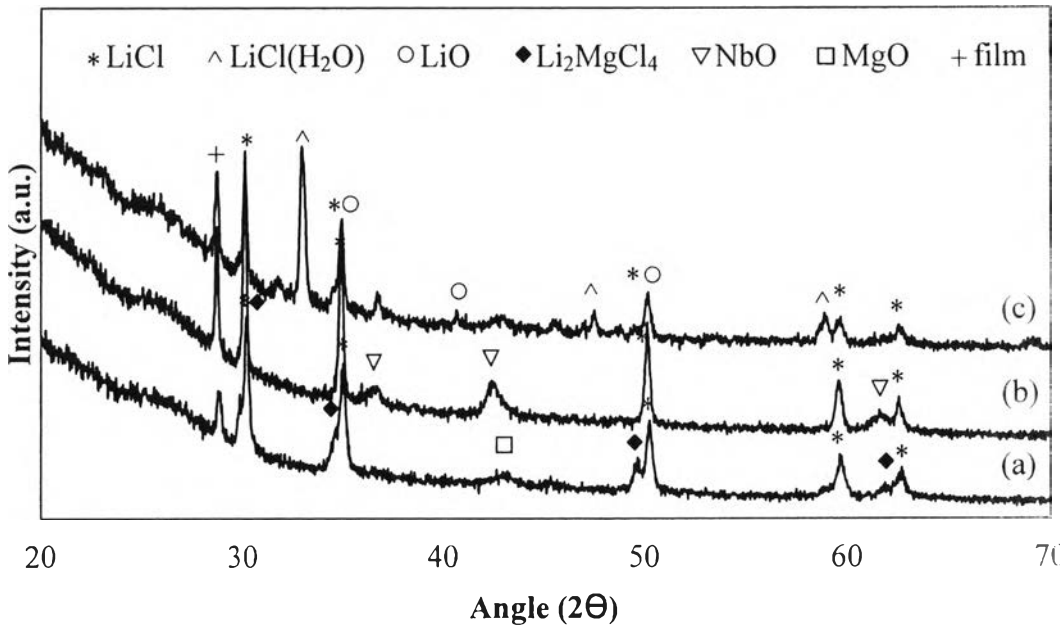

Figure 4.21 X-ray diffraction patterns of 16 wt% $NbCl_5$-$LiBH_4/MgCl_2$ (a), 16 wt% Nb_2O_5-$LiBH_4/MgCl_2$ (b), and X-ray diffraction patterns of the $LiBH_4/MgCl_2$ mixture after the hydrogen desorption (c).

4.2.4 Effects of TiO_2 Amount

The hydrogen desorption of TiO_2-$LiBH_4/MgCl_2$ was investigated at the desorption temperature of 450 °C to identify the optimum amount of TiO_2.

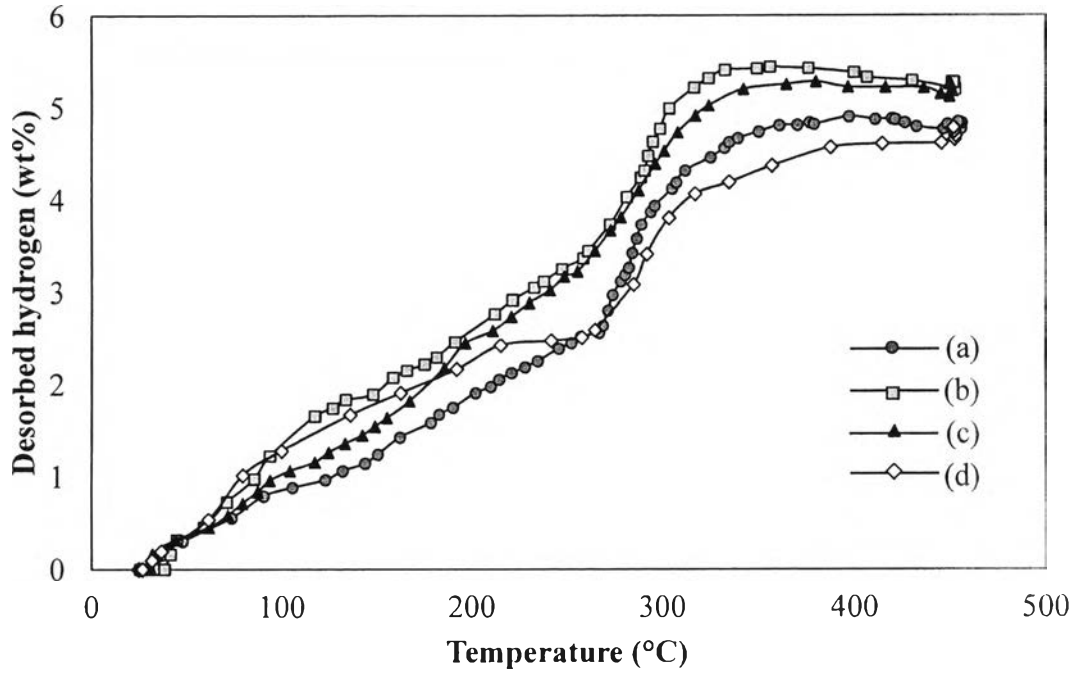

Figure 4.22 Hydrogen desorption profiles of TiO_2-$LiBH_4/MgCl_2$ mixture with different amounts of TiO_2: (a) 10 wt%, (b) 16 wt%, (c) 20 wt% and the $LiBH_4/MgCl_2$ mixture milled for 2 h (d).

The desorption profiles of different amounts of TiO_2 catalyst for 10, 16, and 20 wt% are shown in Figure 4.22. All doped samples release hydrogen in two steps corresponding with the hydrogen desorption of the $LiBH_4/MgCl_2$ mixture. The starting hydrogen desorption temperature of all doped samples are resemble. They release hydrogen around 250 °C for the first step. For the second hydrogen desorption step, 16 wt% TiO_2-$LiBH_4/MgCl_2$ mixture shows the lowest desorption temperature and 10 wt% TiO_2-$LiBH_4/MgCl_2$ mixture shows the highest desorption temperature.

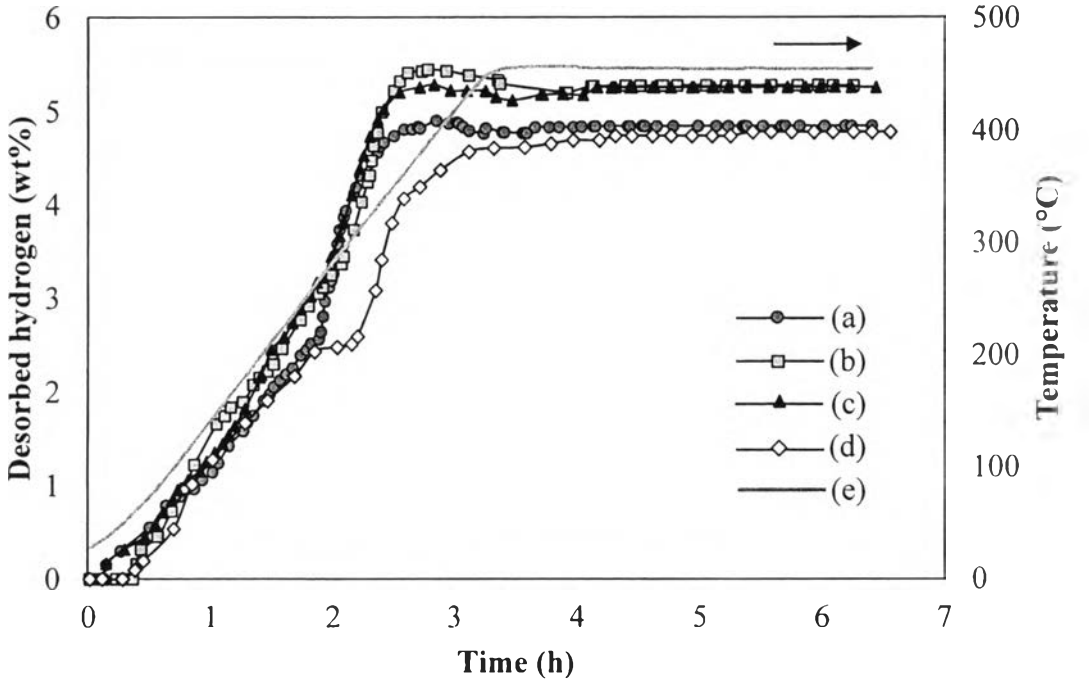

Figure 4.23 Hydrogen desorption profiles as a function of time of TiO_2-$LiBH_4/MgCl_2$ mixture with different amounts of TiO_2: (a) 10 wt%, (b) 16 wt%, (c) 20 wt% and the $LiBH_4/MgCl_2$ mixture milled for 2 h (d) and temperature (e).

From Figure 4.23, it is obvious that the amount of TiO_2 affects the kinetics of the $LiBH_4/MgCl_2$ desorption. Among the tested amounts of TiO_2, using 16 wt% results in the highest initial hydrogen desorption rate and the hydrogen capacity. With 20 wt% TiO_2 catalyst, its desorption profile seems to be close to that with 16 wt% TiO_2. However, the desorbed hydrogen is slightly lower than that with 16 wt% TiO_2 whereas that with 10 wt% TiO_2 shows the hydrogen capacity similar to the undoped sample.

The results of hydrogen desorption with different amounts of TiO_2 are shown in Table 4.4. It is worth noting that high catalyst contents also have a significant effect on kinetics of hydrogen desorption, e.g. 16 and 20 wt% TiO_2 show better results than 10 wt% TiO_2 catalyst. However, Sridechprasat (2011) reported that in terms of hydrogen desorption capacity, the higher amount of a catalyst, the lower the hydrogen desorption capacity.

Table 4.4 Hydrogen desorption temperature and total amount of desorption hydrogen of the $LiBH_4/MgCl_2$ mixture and the mixture doped with different amounts of TiO_2 catalysts after ball milling for 2 h

$LiBH_4/MgCl_2$ mixture	Desorption temperature, °C				Hydrogen capacity, wt%			
	Undoped	10 wt%	16 wt%	20 wt%	Undoped	10 wt%	16 wt%	20 wt%
Step 1	214	251	246	248	2.43	2.45	3.25	3.17
Step 2	374	334	303	317	2.10	2.17	1.74	1.74
Total H_2 (wt%)					4.78	4.84	5.27	5.26

4.2.5 Effects of Nb_2O_5 Amount

The influence of Nb_2O_5 amounts on the hydrogen desorption kinetics of $Mg(BH_4)_2$ was also investigated at the desorption temperature of 450 °C. In general, an increase in the Nb_2O_5 amounts has a positive effect on the desorption kinetics. For example, it was reported that the fastest kinetics of the magnesium hydrogen sorption are obtained using 0.5 mole% Nb_2O_5, (Barkhordarian *et al.*, 2003).

The hydrogen desorption profiles of Nb_2O_5-$LiBH_4/MgCl_2$ mixture with different amounts of Nb_2O_5 are shown in Figure 4.24. The desorption profiles of 10 and 20 wt% Nb_2O_5-$LiBH_4/MgCl_2$ mixture show that it is difficult to identify the desorption temperature in each step. The reason may be the reaction between $LiBH_4$ and $MgCl_2$ does not complete during the ball milling process. Hydrogen evolved from the decomposition of 10, 16, and 20 wt% Nb_2O_5 in the $LiBH_4/MgCl_2$ mixture are 4.58, 4.86, and 4.71 wt%, respectively.

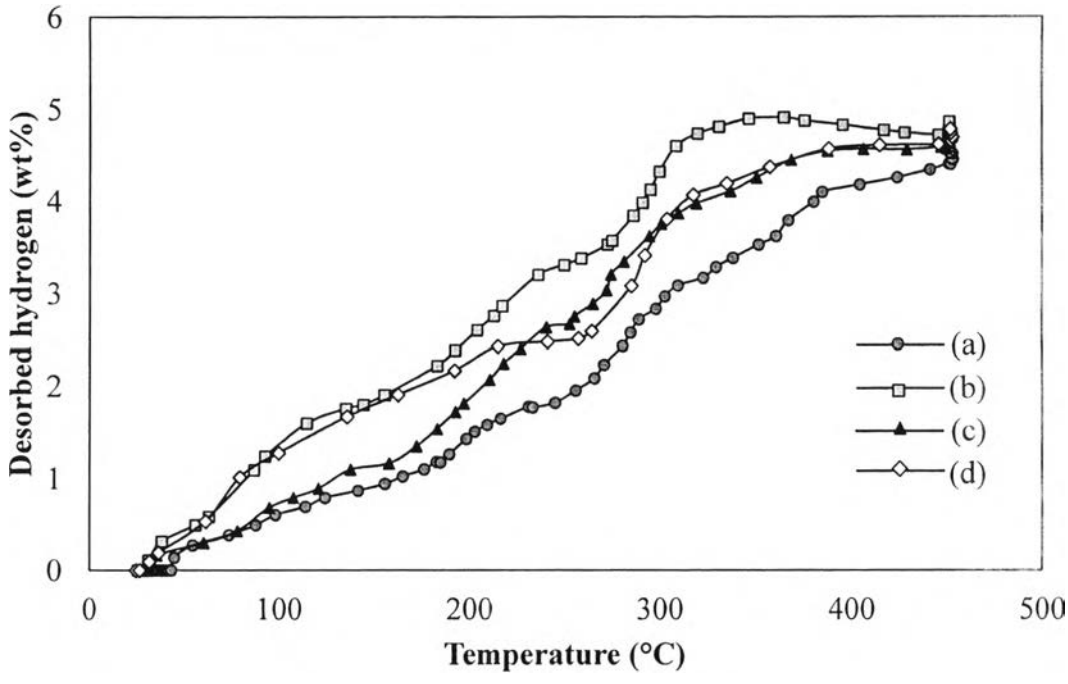

Figure 4.24 Hydrogen desorption profiles of Nb_2O_5-$LiBH_4/MgCl_2$ mixture with different amounts of Nb_2O_5: (a) 10 wt%, (b) 16 wt%, (c) 20 wt% and the $LiBH_4/MgCl_2$ mixture milled for 2 h (d).

The desorption rates of the Nb_2O_5-$LiBH_4/MgCl_2$ mixture with different amounts of Nb_2O_5 are shown as hydrogen desorption profiles in Figure 4.25. In the initial period of the desorption process, the addition of 10 and 20 wt% of Nb_2O_5 (Figure 4.25(a), (c)) lowers the desorption for the undoped sample, whereas 16 wt% of Nb_2O_5 (Figure 4.25(b)) shows the best performance for the $LiBH_4/MgCl_2$ mixture desorption. As mentioned before, an increase in the Nb_2O_5 amount has a positive effect on the desorption kinetics (Barkhordarian *et al.*, 2003). However, the results demonstrate that further for the increase in the amount of Nb_2O_5 catalyst results in an adversed effect on the reaction kinetics. The possible reason could be a saturation limit is reached for 16 wt% of Nb_2O_5 and kinetics cannot be accelerated further with the further increase in the catalyst amount. This is also consistent with a report by Barkhordarian *et al.* (2003).

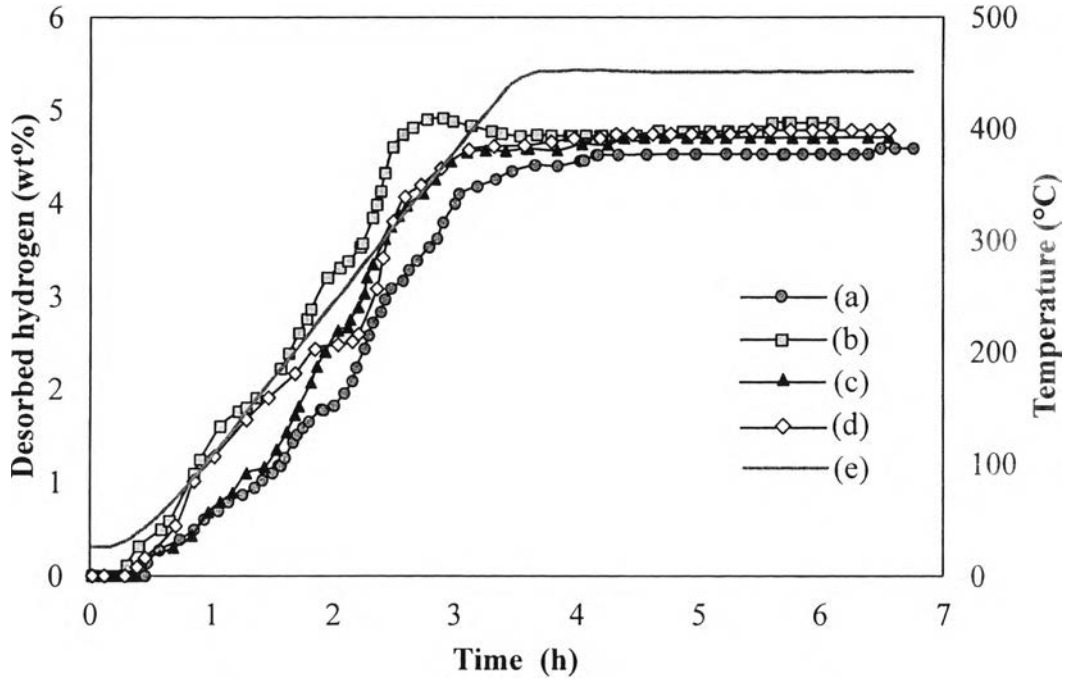

Figure 4.25 Hydrogen desorption profiles as a function of time of Nb_2O_5-$LiBH_4/MgCl_2$ mixture with different amounts of Nb_2O_5: (a) 10 wt%, (b) 16 wt%, (c) 20 wt% and the $LiBH_4/MgCl_2$ mixture milled for 2 h (d) and temperature (e).

4.3 Hydrogen Absorption of $Mg(BH_4)_2$

The absorption reaction of the dehydrided $LiBH_4/MgCl_2$ mixture was conducted with the thermo-volumetric apparatus at 350 °C under 9.5 MPa hydrogen pressure for 12 h. All samples show similar results. That is, after the absorption process, hydrogen pressure is the same as before the rehydriding reaction and the desorbed quantity of hydrogen is miniscule. Therefore, the dehydrided $LiBH_4/MgCl_2$ mixture milled for 2 and 5 h and the dehydrided $LiBH_4/MgCl_2$ samples mixed with Ti- and Nb-based catalysts cannot absorb hydrogen. The results are similar to Varin and Zbroniec (2010), who investigated the re-absorption of $LiBH_4/MnCl_2$ under pressure of 10 MPa hydrogen for 12 h, and showed that the system was most likely irreversible. However, a previous report Li *et al.* (2008) shows the Raman spectra of dehydrided $Mg(BH_4)_2$ that revealed the vibrating modes of the B-H bonding. This

suggests that the formation of a new Mg-B-H compound along with the progress of the rehydriding reaction.

Furthermore, some information in the literature on the properties of $Mg(BH_4)_2$ were reported by infrared spectroscopy (FTIR). Typical features of the BH_4 group can be observed in the IR spectra, i.e. the stretching and deformation of B-H bonds in the regions between 2150 and 2400 cm^{-1} and 1100 and 1300 cm^{-1}, respectively (Chlopek *et al.*, 2007). Figure 4.26 shows the FTIR spectra of the $LiBH_4/MgCl_2$ mixture after desorption and re-absorption. They show similar transmission bands. For the desorbed $LiBH_4/MgCl_2$ mixture, the presence of transmission bands around 2441 and 1558 cm^{-1} that are beyond the regions of B-H bonds. Therefore, after the desorption process, the B-H bond is destroyed.

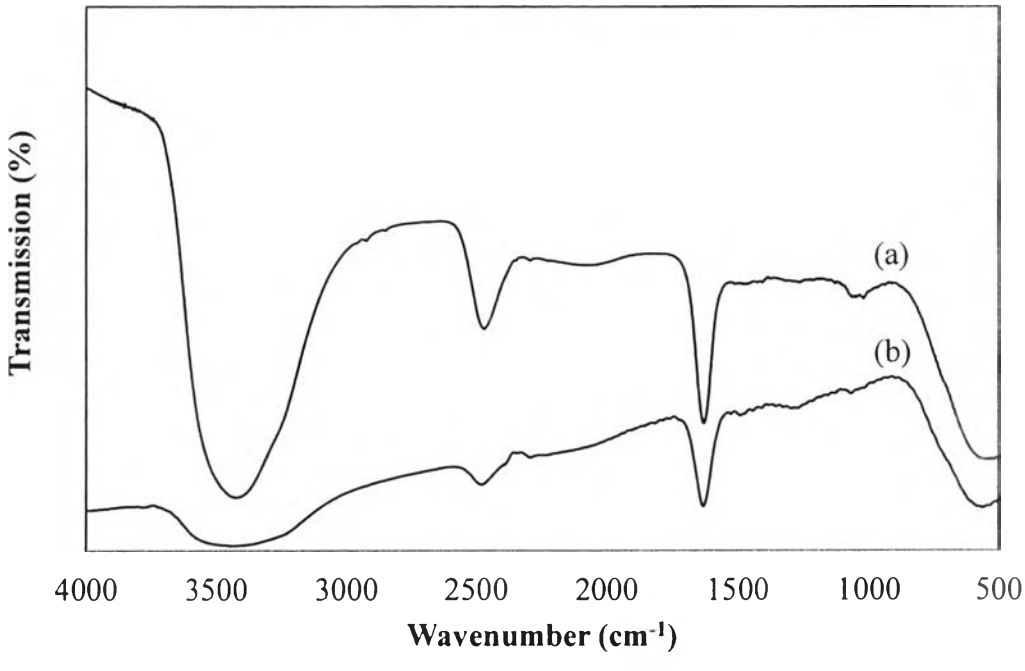

Figure 4.26 FTIR spectra of the $LiBH_4/MgCl_2$ mixture milled for 2 h after desorption at 450 °C (a), and after re-absorption at 350 °C for 12 h (b).

It is well-known that the reversible reaction of metal hydrides is improved when a catalyst such as Ti-and Nb-based catalysts is applied (Sridechprasat, 2011 and Fan *et al.*, 2008). However, results from the FTIR spectra (Figures 4.26 and 4.27) show that there are no transmission bands in the range of the B-H bonds. TiO_2-

$LiBH_4/MgCl_2$ mixture after re-absorption (Figure 4.26(a)) shows the transmission band around 2433 and 1616 cm^{-1}, respectively.

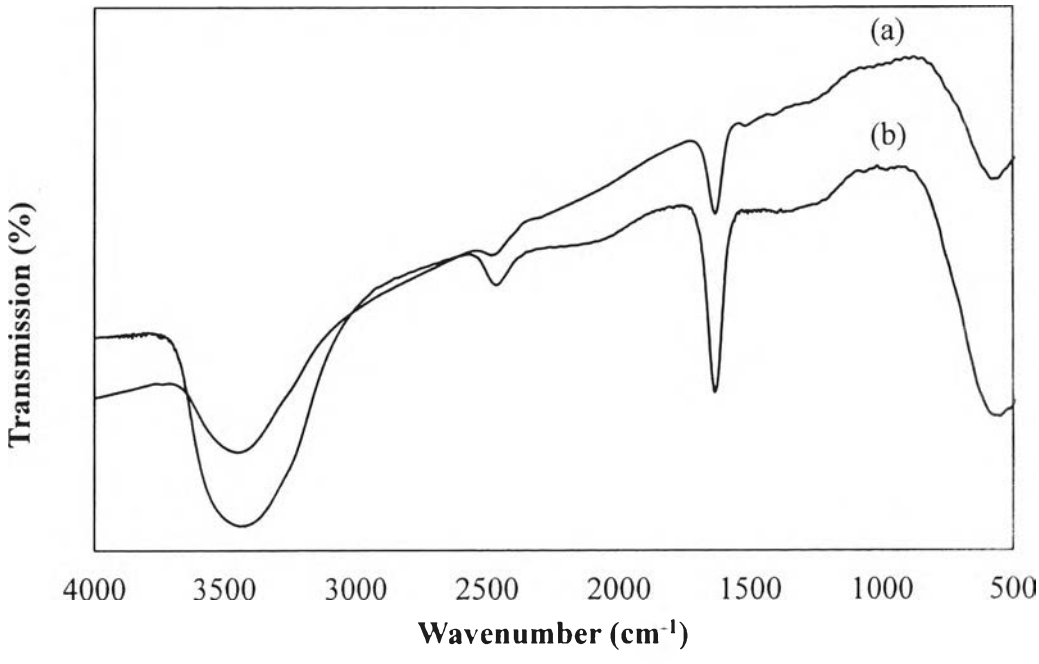

Figure 4.27 FTIR spectra of TiO_2-$LiBH_4/MgCl_2$ mixture milled for 2 h after desorption at 450 °C (a), and after re-absorption at 350 °C for 12 h (b).

In addition, the FTIR spectra of Nb_2O_5-$LiBH_4/MgCl_2$ mixture also show similar transmission bands to the undoped sample and the one doped with TiO_2. It can be seen in Figure 4.27(b) that the transmission bands of Nb_2O_5 doped sample after the re-absorption appear at 2435 and 1600 cm^{-1}. The transmission bands of both samples (Figure 4.27) show similar results and are not in the regions of B-H bonds. Therefore, TiO_2 and Nb_2O_5 catalysts cannot improve the reversible reaction of the $LiBH_4/MgCl_2$ mixture.

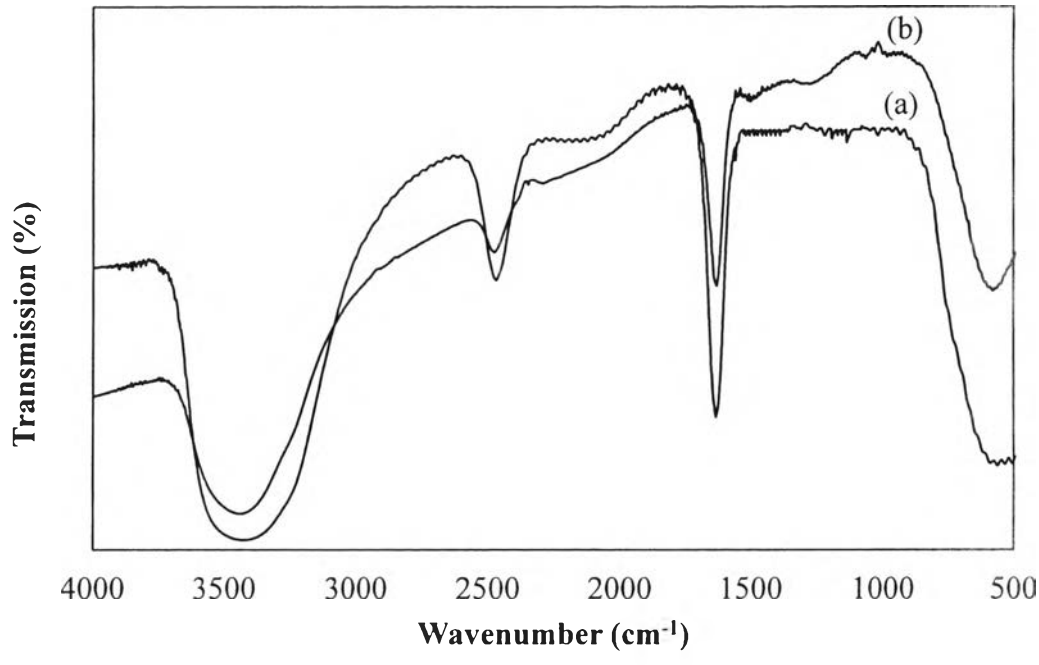

Figure 4.28 FTIR spectra of Nb_2O_5-$LiBH_4$/$MgCl_2$ mixture milled for 2 h after desorption at 450 °C (a), and after re-absorption at 350 °C for 12 h (b).